Effect of ultrastrong magnetic fields on laser-produced gamma-ray flashes

P. Hadjisolomou,[1,*] R. Shaisultanov,[1] T. M. Jeong,[1] P. Valenta,[1] and S. V. Bulanov[1,2]

[1]*ELI Beamlines Facility, Extreme Light Infrastructure ERIC, Za Radnicí 835, 25241 Dolní Břežany, Czech Republic*

[2]*National Institutes for Quantum Science and Technology (QST), Kansai Photon Science Institute, 8-1-7 Umemidai, Kizugawa, Kyoto 619-0215, Japan*

(Received 27 June 2023; accepted 27 September 2023; published 15 November 2023)

Laser produced γ-photons can make an important impact on applied and fundamental physics that require high γ-photon yield and strong collimation. We propose the addition of a constant magnetic field to the laser-solid interaction to obtain the aforementioned desired γ-photon properties. The γ-ray flash spatial and spectral characteristics are obtained via quantum electrodynamic particle-in-cell simulations. When the constant magnetic field aligns with the laser magnetic field, then the γ-ray emission is significantly enhanced. Moreover, the γ-photon spatial distribution becomes collimated, approximately in the form of a disk.

DOI: 10.1103/PhysRevResearch.5.043153

The 1980s witnessed the invention of the chirped pulse amplification technique [1], which resulted in the rapid growth of laser power, exceeding the petawatt (PW) level by the end of the 20th century [2]. The 10 PW lasers [3] became a reality with a femtosecond-class laser in ELI-NP (surpassing the CoReLS 4 PW laser), another laser of ten times higher energy being near completion in ELI-Beamlines, the upgrade of the Apollon laser, and the commissioning of the SULF laser [4].

When a PW-class laser interacts with matter, energetic charged particles are generated; this was the norm over many years. Once multi-PW laser facilities came into existence, the generation and usage of γ-photons became one of their main tasks. A high laser to γ-photon energy conversion efficiency, κ_γ, is predicted [5–7]. The γ-ray flashes are suited to, among others, photonuclear reactions [8], positron sources [9], neutron sources [10], extreme energy density materials science [11], and studies on fundamental processes [12].

The γ-ray flash is a result of the multiphoton Compton scattering process [13], which occurs when an electron collides with a laser, emitting a scattered γ-photon. The scattering process is expressed as $e^- + N_l\omega_l \rightarrow e^- + \omega_\gamma$, where e^- represents an electron, $N_l \gg 1$ is the number of laser photons, ω_l is the laser frequency, and ω_γ is the scattered γ-photon frequency. The γ-photon yield is quantified by the quantum nonlinearity parameter, $\chi_e = \gamma_e E_S^{-1}\sqrt{(\mathbf{E}+\mathbf{v}\times\mathbf{B})^2 - (\mathbf{v}\cdot\mathbf{E}/c)^2}$. Here, $E_S = m_e^2c^3/(e\hbar) \approx 1.3\times10^{18}\,\mathrm{V\,m^{-1}}$ is the Schwinger field (m_e is the electron rest mass, c is the vacuum speed of light, e is the elementary charge, and $\hbar$ is the reduced Planck constant), γ_e is the Lorentz factor of an electron with velocity $\mathbf{v}$ before scattering, $\mathbf{E}$ is the electric field, and $\mathbf{B}$ is the magnetic field. High κ_γ values require $\chi_e \gg 1$ [5,6].

The purpose of this paper is to demonstrate that a constant magnetic field (CMF) added to a laser field can enhance the γ-photon yield and directionality from laser-solid interactions. Initially we study the single-electron dynamics under the effect of an ultraintense laser in addition to a CMF, with radiation reaction force taken into account. We then extend our study to particle-in-cell (PIC) simulations with the target being a lithium slab, as shown in Fig. 1. It has recently been shown that lithium combined with multi-PW lasers results in high κ_γ [14]; although the generation of a small electron-positron pair population through the multiphoton Breit-Wheeler process is possible under the conditions examined, it does not affect the γ-photon emission and is therefore ignored. We demonstrate that a strong CMF orthogonal to the laser propagation direction increases κ_γ by several times. Moreover, if the CMF aligns with the laser magnetic field, then the γ-ray flash distribution resembles a narrow disk along the laser electric field oscillating plane, increasing the fluence of the emitted γ-photon.

Let us measure velocity in c, momentum in m_ec, distance in $\lambda\!\!\!^{-} = \lambda/(2\pi)$ (where $\lambda = 0.815\,\mu\mathrm{m}$ is the laser wavelength), and time in ω_l^{-1} (where $\omega_l = c/\lambda\!\!\!^{-}$). We use a linearly polarized electromagnetic wave with an electric field $\boldsymbol{E}_l = [0, a\cos(t-x), 0]$ and a magnetic field $\boldsymbol{B}_l = [0, 0, ac^{-1}\cos(t-x)]$. The normalized dimensionless amplitude of the wave is $a = eE_l/(m_ec\omega_l) \approx 350$. The normalized dimensionless amplitude of the CMF, $\boldsymbol{\mathcal{B}}$, is $\boldsymbol{b} = e\boldsymbol{\mathcal{B}}/(m_e\omega_l) = [b_x, b_y, b_z]$, and its effect on the electron motion is studied for the values of 75, 150, and 300. These fields are in the megatesla scale for the wavelength under consideration [15–17].

A radiation reaction force, $\boldsymbol{F}_{\mathrm{rad}} = -\boldsymbol{p}2am_ec^2\chi_e^2G_e/(3\hbar\gamma_e)$, is considered [18], where $\boldsymbol{p} = [p_x, p_y, p_z]$ is the electron momentum and $G_e = (1 + 8.93\chi_e + 2.41\chi_e^2)^{-2/3}$ is the Gaunt factor, which accounts for quantum electrodynamics correction of the radiation reaction effect [7]. The equations of

*Prokopis.Hadjisolomou@eli-beams.eu

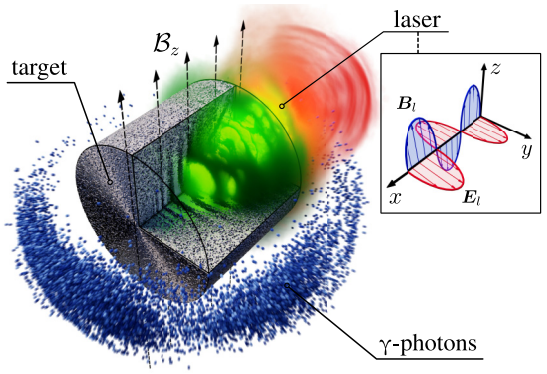

FIG. 1. An $a = 350$ laser (figure inset) interacting with a lithium foil in the presence of a CMF (black dashed arrows) at 80 fs PIC simulation time. The case in which the CMF corresponds to the $b_z = 150$ case is depicted. The laser-foil interaction results in enhanced γ-photon emission, illustrated by blue spheres (energy larger than $500\, m_e c^2$, with a ballistic offset of 10 μm). The green-red and gray show the laser field and the target, respectively.

motion are

$$\frac{d\boldsymbol{r}}{dt} = \frac{\boldsymbol{p}}{\gamma_e} \tag{1}$$

and

$$\frac{d\boldsymbol{p}}{dt} = -\left[\boldsymbol{E}_l + \frac{\boldsymbol{p}}{\gamma_e} \times (c\boldsymbol{B}_l + \boldsymbol{b}) + \frac{2\alpha m_e c^2}{3\hbar\omega_l}\chi_e^2 G_e \frac{\boldsymbol{p}}{\gamma_e}\right]. \tag{2}$$

Here, $\boldsymbol{r} = [x, y, z]$, $\alpha = e^2/(4\pi\varepsilon_0\hbar c)$ is the fine-structure constant, and ε_0 is the vacuum permittivity.

The obtained single-electron trajectories are shown in Figs. 2(a)–2(d) and Figs. 3(a)–3(d). Figures 2(a) and 3(a) correspond to the reference case in which only a plane electromagnetic wave is considered [19], without CMF. The electron drifts along the x-axis with a drift velocity, $u_d \lesssim c$; the electron trajectory in the electron average rest frame is a figure-eight. The radiation reaction force is maximized where the trajectory curvature is high. Projection of electron trajectories at those locations indicates that the radiation is emitted at two symmetric lobes [5,14].

Let us set $b = 150$, except where otherwise mentioned. For the b_x case [see Fig. 2(b)], the electron trajectory forms periodic spiral-like patterns, with the period decreasing for increasing b_x. The ratio of its z-axis to y-axis extent is b_x. The radiation reaction force initially obtains low values of $0.0018 m_e c\omega_l$ and they slowly decrease thereafter. The particle trajectory is approximately the same whether or not the radiation reaction is considered, with $\gamma \approx 12$. Note that the b_x case combined with a circularly polarized laser in the absence of radiation reaction was studied six decades ago. It was referred to as the autoresonance effect, where an electron can be accelerated to high energies [20,21]. However, the inclusion of the radiation reaction suppresses the autoresonance scheme [22,23].

For the b_y case [see Fig. 2(c)], the electron propagation direction rotates approximately -12° (for the parameters defined) on the xz-plane. By shifting the electron trajectory along the new propagation axis, the trajectories form figure-eight patterns, with the trajectory period decreasing for

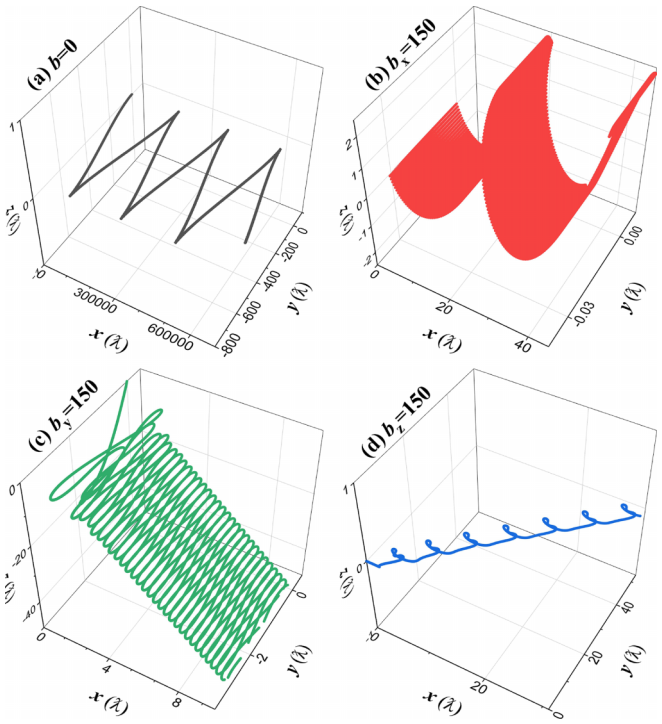

FIG. 2. Electron trajectory by solving equations of motion under the influence of a linearly polarized electromagnetic wave of $a \approx 350$ plus a CMF of (a) $b = 0$, (b) $b_x = 150$, (c) $b_y = 150$, and (d) $b_z = 150$.

increasing b_y. Thus, the highest γ-photon energy yield is expected at two lobes located at negative z-values. The Lorentz factor obtains a peak value of $\gamma \approx 390$, while the radiation reaction force reaches values of $\approx 55 m_e c\omega_l$, revealing strong γ-photon emission.

If the radiation reaction is ignored, the b_z case gives circular trajectories along the xy-plane, as shown in Fig. 3(b), passing through $z = 0$ and symmetrically around the y-axis; no drifting of the electron trajectory occurs [24]. In this case, the Lorentz factor is $O(10^3)$. The picture changes by the inclusion of radiation reaction, where the electron trajectory drifts along an axis (with $u_d \approx 0.518$) forming an angle $\theta \approx \arccos(1 - b_z/a) \approx 55^\circ$ with the laser propagation axis. The electron trajectories form periodic high-curvature patterns, as shown in Figs. 2(d) and 3(c). By considering the electron average rest frame, a heart-shaped figure is revealed, as seen in Fig. 3(d). The Lorentz factor peaks at $\gamma \approx 1440$, with a period matching that of the high-curvature patterns. The b_z case corresponds to the highest radiation reaction force values, at $\approx 320 m_e c\omega_l$, and the strongest γ-photon emission is expected for this case. Due to the electron trajectory restricted on the xy-plane, all γ-photons are emitted as a γ-ray disk.

Now we realize the laser-target interaction through three-dimensional relativistic quantum electrodynamic PIC simulations. We use the EPOCH [25,26] code, enabling the Photons (acknowledging the radiation reaction effect) and the Higuera-Cary (obtaining accurate high-energy electron trajectories) preprocessor directives. For similar interaction parameters, in the absence of the CMF, Compton γ-photons dominate

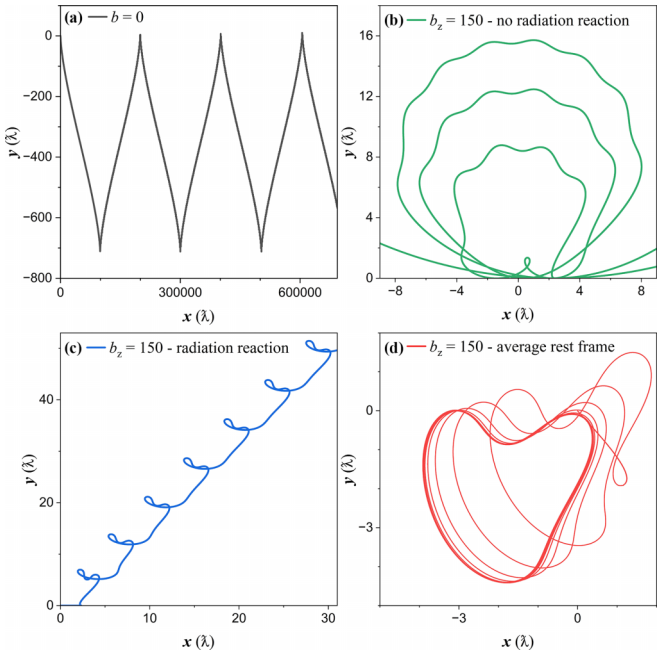

FIG. 3. Electron trajectory by solving equations of motion under the influence of a linearly polarized electromagnetic wave of $a \approx 350$ plus a CMF of (a) $b = 0$, (b) $b_z = 150$ ignoring radiation reaction, (c) $b_z = 150$ including radiation reaction, and (d) $b_z = 150$ including radiation reaction, in electron average rest frame.

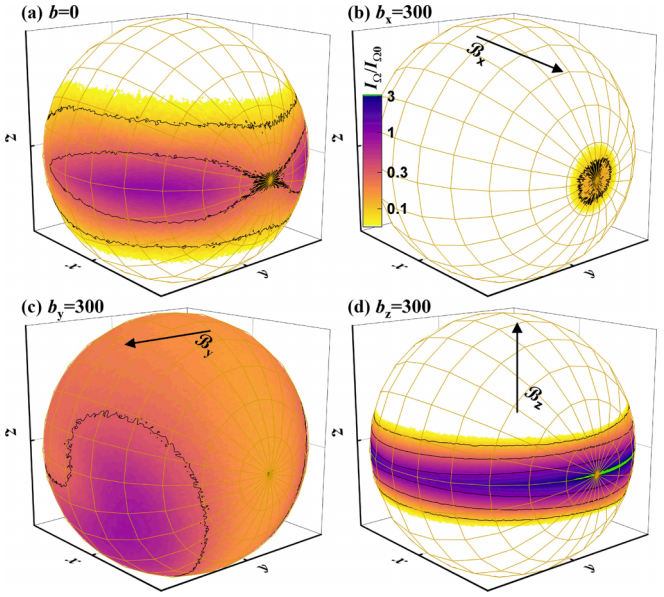

FIG. 4. $I_\Omega/I_{\Omega 0}$ as obtained by PIC simulations of an $a = 350$ laser interacting with a lithium target in the presence of a CMF, for the cases of (a) $b = 0$, (b) $b_x = 300$, (c) $b_y = 300$, and (d) $b_z = 300$. For the $b_z = 300$ case, the color bar saturates (green).

over bremsstrahlung γ-photons within the simulation time [14]. Therefore, the bremsstrahlung preprocessor directive is not enabled. Although a small population of electron-positron pairs (orders of magnitude smaller than the target electrons) is generated during the interaction [14], they are ignored as we are only interested in the γ-ray flash characterization.

The laser and CMF parameters used in the PIC simulations match those used in the single-electron model, where now the pulsed nature of the laser is considered with a 17λ̄ focused diameter, $40\omega_l^{-1}$ pulse duration, and a pulse temporal offset of two standard deviations. Three simulation sets are performed, each having the CMF oriented along one of the three Cartesian axes. The laser focuses in the center of the simulation box, with box open boundaries at ± 15.36 μm in each direction. Normal laser incidence on the target (yz-plane) requires 10 nm cells along the x-axis and 40 nm on the other two, where eight macroelectrons and eight macroions are assigned per cell. The laser peak reaches the focal spot at 65 fs, while it requires 110 fs for γ-photon emission to increase asymptotically, indicating that Compton γ-photon emission occurs in timescales comparable to the laser duration.

The γ-photon radiant intensity, I_Ω, being the total γ-photon energy emitted per solid angle per pulse duration, maps the γ-photon directionality. The $b = 0$ case corresponds to a peak I_Ω reference value of $I_{\Omega 0}$. Figures 4(a)–4(d) depict $I_\Omega/I_{\Omega 0}$, with the CMF orientation labeled in the figure. Figure 4(a) shows a γ-photon double-lobe structure, as predicted by previous PIC simulations and in agreement with our single-electron model.

Figure 4(b) corresponds to the b_x case, where weak radiation reaction effects occur, and peak I_Ω is more than three times lower than the $b = 0$ case. The radially symmetric distribution of the γ-photons geometrically result in a collimated γ-ray flash along the laser propagation axis. The b_y case shown in Fig. 4(c) has peak I_Ω comparable (within 10%) to $I_{\Omega 0}$. However, the lobes are enlarged, revealing a larger κ_γ value.

The γ-ray disk reappears in Fig. 4(d), corresponding to the b_z case. Here, the γ-photons pile up on a narrow distribution on the xy-plane. Projection of the electron trajectories [see Figs. 2(d) and 3(c)] suggests that the γ-ray disk is not uniform along the xy-plane. For the $b_z \approx 300$ case, a lobe of $I_\Omega/I_{\Omega 0} > 3$ occurs, squeezed within an angle of $<10^\circ$ at full width at half-maximum along the z-axis.

Our results, expanded over a CMF amplitude range, are summarized in Fig. 5. The b_x, b_y, and b_z cases are represented by the blue, green, and red lines, respectively. The continuous

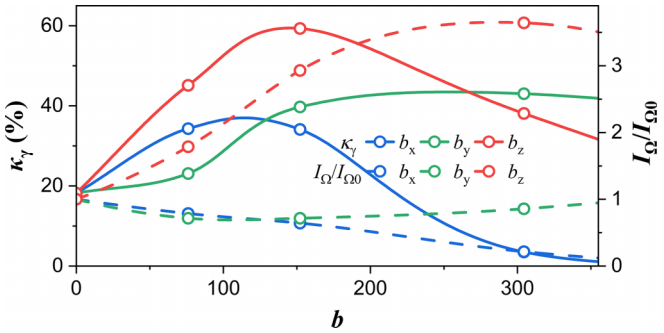

FIG. 5. Left axis, solid lines: κ_γ as a function of b, due to the interaction of an $a = 350$ laser with a lithium foil in the presence of a CMF. b_x, b_y, and b_z correspond to the blue, green, and red lines, respectively, reaching a κ_γ value of 60% for the $b_z \approx 150$ case. Right axis, dashed lines: peak $I_\Omega/I_{\Omega 0}$ as a function of b.

lines show κ_γ as a function of b. If no magnetic field is applied, the laser interaction with the lithium target results in $\kappa_\gamma \approx 20\%$. For the b_x case, applying a CMF up to $b_x \approx 150$ increases κ_γ, but a further increase of b_x results in a rapid decrease of κ_γ. This effect is due to magnetically induced transparency of the target [27], where a highly transparent target results in weak laser-target interaction, therefore low γ-photon emission. The dashed blue line shows $I_\Omega/I_{\Omega 0}$ steadily decreasing for increasing b_x.

Our PIC simulations reveal that magnetically induced transparency does not occur if the CMF is along the y-axis, within our parameters of interest. Although $I_\Omega/I_{\Omega 0}$ remains approximately constant, the extent of the γ-photon lobes increases. As a result, κ_γ gradually increases, reaching $\kappa_\gamma \approx 40\%$ for $b_y = 300$.

Target transparency also occurs for the b_z case [28–30], where $b_z > 150$ results in a decrease of κ_γ. However, at $b_z = 150$ we obtain $\kappa_\gamma \approx 60\%$, three times higher than the reference case. The b_z case is of particular interest also due to its high I_Ω, as seen by the red dashed line in Fig. 5(a). Although optimal κ_γ occurs at $b_z = 150$, optimal $I_\Omega/I_{\Omega 0}$ occurs at $b_z = 300$ due to a narrower (along the z-axis) γ-photon lobe.

The γ-photon energy spectrum depends on the γ-photon detection angle. This is seen in Fig. 6(a), where the normalized fluence is shown, for the three b_z cases examined as labeled in the figure. For the $b = 0$ case, two symmetric lobes are obtained. However, by increasing the CMF value the first lobe shifts closer to the laser propagation axis while the second shifts far from the axis. In addition, the figure depicts with the blue shadowed region the case in which only γ-photons of energy larger than $500 m_e c^2$ are considered. There, a dominant lobe exists on the laser propagation axis with a divergence of approximately 10° at full width at half-maximum, and another less prominent lobe at angles of -45°, -65°, and -110° for the $b_z = 75$, 150, and 300 cases, respectively.

For applications, one needs to know how the γ-photon number changes per energy interval. Therefore, we calculate the ratio of the γ-photon spectrum at the peak I_Ω location for the b_z case to the reference case. For $b_z = 150$, I_Ω peaks at 20° to the laser propagation axis, and for $b_z = 300$ it peaks at 15°; for $b = 0$, the reference I_Ω peaks at 45°. The spectra ratios for the $b_z = 150$ and 300 cases are shown in Fig. 6(b) with red and blue lines, respectively. In both cases, the γ-photon number, N_γ, is increased three (for higher γ-photon energies) to five (for lower γ-photon energies) times compared to the reference γ-photon number, $N_{\gamma 0}$. However, considering peak I_Ω only of higher energy γ-photons results in spectra ratios as shown in Fig. 6(c). The lobe on the laser propagation axis contains approximately twice as high energy γ-photons compared to the reference case, taken at 50°. The second lobe contains approximately the same number of high-energy γ-photons as in the reference case.

In conclusion, the spatial and spectral distributions of the emitted γ-photons are obtained via PIC simulations, where an $a = 350$ laser interacts with a lithium foil. The radiation reaction force alters the trajectory of a single electron moving under the influence of an ultraintense laser in addition to a CMF. The radiation reaction force obtains high values when the CMF is transverse to the laser propagation axis. If the

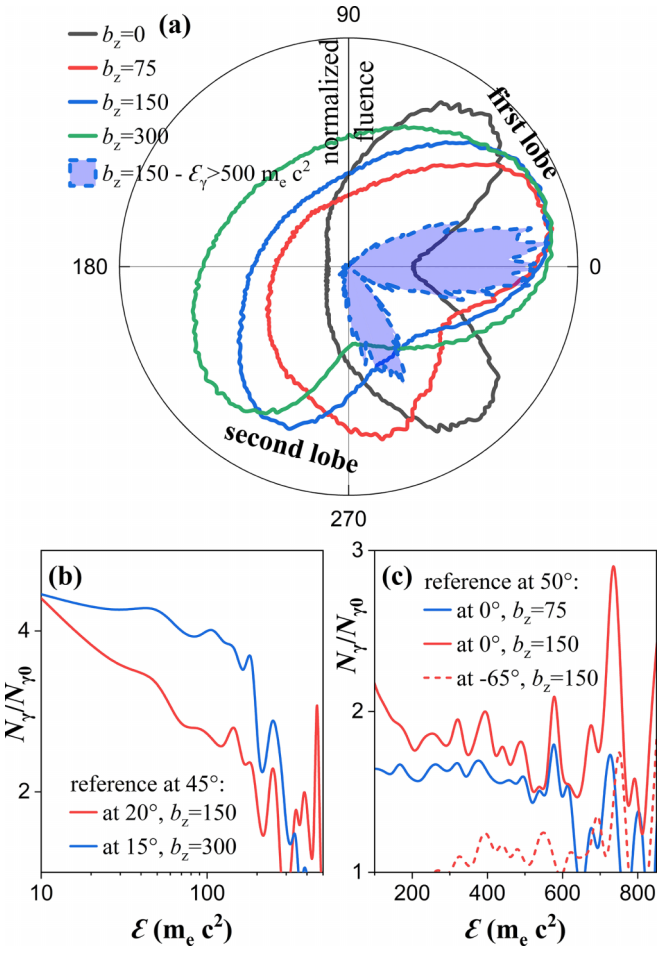

FIG. 6. (a) Normalized fluence in radial directions on the xy-plane, within 1° full angle. The cases $b = 0$, $b_z = 75$, $b_z = 150$, and $b_z = 300$ correspond to the black, red, blue, and green lines, respectively. The blue filled area corresponds to the $b_z = 150$ case by considering only γ-photons of energy larger than $500 m_e c^2$. (b) The ratio of b_z to $b = 0$ γ-photon energy spectra, measured at peak I_Ω within a 1° full angle. (c) The ratio of b_z to $b = 0$ γ-photon energy spectra, measured at peak I_Ω (where here for I_Ω we consider only γ-photons of energy larger than $500 m_e c^2$), within a 10° full angle. The $b_z \approx 150$ and $b_z \approx 300$ cases correspond to the red and blue lines, respectively.

CMF aligns with the laser electric field, then the γ-photons are emitted in two broad lobes, while if it coincides with the laser magnetic field, then the electron moves strictly on the xy-plane and the γ-photons are emitted mostly along that plane. Specifically, the radiant intensity for the $b_z = 300$ case is increased by a factor of more than 3. The highest κ_γ is obtained for the $b_z = 150$ case, reaching up to 60%, three times higher than the reference case. Moreover, the amplitude of the lower and higher part of the γ-photon energy spectrum is increased by a factor of 5 and 2, respectively. The enhancement of the low-energy γ-photon number at optimal emission angles suits photonuclear reactions [8]. The higher-energy γ-photon number is doubled along the laser propagation axis, necessary for electron-positron pair generation by the nonlinear Breit-Wheeler process [12].

This work is supported by the project "Advanced research using high intensity laser produced photons and particles" (ADONIS) (CZ.02.1.01/0.0/0.0/16 019/0000789) from the European Regional Development Fund and by the Ministry of Education, Youth and Sports of the Czech Republic through the e-INFRA CZ (ID:90254). The EPOCH code is funded in part by the UK EPSRC Grants No. EP/G054950/1, No. EP/G056803/1, No. EP/G055165/1, and No. EP/M022463/1.

[1] D. Strickland and G. Mourou, Compression of amplified chirped optical pulses, Opt. Commun. **56**, 219 (1985).

[2] M. D. Perry, D. Pennington, B. C. Stuart, G. Tietbohl, J. A. Britten, C. Brown, S. Herman, B. Golick, M. Kartz, J. Miller *et al.*, Petawatt laser pulses, Opt. Lett. **24**, 160 (1999).

[3] C. N. Danson, C. Haefner, J. Bromage, T. Butcher, J. F. Chanteloup, E. A. Chowdhury, A. Galvanauskas, L. A. Gizzi, J. Hein, and D. I. e. a. Hillier, Petawatt and exawatt class lasers worldwide, High Power Laser Sci. Eng. **7**, e54 (2019).

[4] A. X. Li, C. Y. Qin, H. Zhang, S. Li, L. L. Fan, Q. S. Wang, T. J. Xu, N. W. Wang, L. H. Yu, Y. Xu *et al.*, Acceleration of 60 MeV proton beams in the commissioning experiment of the SULF-10 PW laser, High Power Laser Sci. Eng. **10**, e26 (2022).

[5] T. Nakamura, J. K. Koga, T. Z. Esirkepov, M. Kando, G. Korn, and S. V. Bulanov, High-power γ-ray flash generation in ultraintense laser-plasma interactions, Phys. Rev. Lett. **108**, 195001 (2012).

[6] C. P. Ridgers, C. S. Brady, R. Duclous, J. G. Kirk, K. Bennett, T. D. Arber, A. P. L. Robinson, and A. R. Bell, Dense electron-positron plasmas and ultraintense γ rays from laser-irradiated solids, Phys. Rev. Lett. **108**, 165006 (2012).

[7] A. Gonoskov, T. G. Blackburn, M. Marklund, and S. S. Bulanov, Charged particle motion and radiation in strong electromagnetic fields, Rev. Mod. Phys. **94**, 045001 (2022).

[8] D. Kolenatý, P. Hadjisolomou, R. Versaci, T. M. Jeong, P. Valenta, V. Olšovcová, and S. V. Bulanov, Electron-positron pairs and radioactive nuclei production by irradiation of high-Z target with γ-photon flash generated by an ultra-intense laser in the λ^3 regime, Phys. Rev. Res. **4**, 023124 (2022).

[9] G. Sarri, K. Poder, J. M. Cole, W. Schumaker, A. Di Piazza, B. Reville, T. Dzelzainis, D. Doria, L. A. Gizzi, G. Grittani, S. Kar, C. H. Keitel, K. Krushelnick, S. Kuschel, S. P. D. Mangles, Z. Najmudin, N. Shukla, L. O. Silva, D. Symes, A. G. R. Thomas *et al.*, Generation of neutral and high-density electron–positron pair plasmas in the laboratory, Nat. Commun. **6**, 6747 (2015).

[10] I. Pomerantz, E. McCary, A. R. Meadows, A. Arefiev, A. C. Bernstein, C. Chester, J. Cortez, M. E. Donovan, G. Dyer, E. W. Gaul, D. Hamilton, D. Kuk, A. C. Lestrade, C. Wang, T. Ditmire, and B. M. Hegelich, Ultrashort pulsed neutron source, Phys. Rev. Lett. **113**, 184801 (2014).

[11] B. Eliasson and C. S. Liu, An electromagnetic gamma-ray free electron laser, J. Plasma Phys. **79**, 995 (2013).

[12] A. J. MacLeod, P. Hadjisolomou, T. M. Jeong, and S. V. Bulanov, All-optical nonlinear Breit-Wheeler pair production with γ-flash photons, Phys. Rev. A **107**, 012215 (2023).

[13] V. I. Ritus, Quantum effects of the interaction of elementary particles with an intense electromagnetic field, J. Sov. Laser Res. **6**, 497 (1985).

[14] P. Hadjisolomou, T. M. Jeong, and S. V. Bulanov, Towards bright gamma-ray flash generation from tailored target irradiated by multi-petawatt laser, Sci. Rep. **12**, 17143 (2022).

[15] M. Tatarakis, I. Watts, F. N. Beg, E. L. Clark, A. E. Dangor, A. Gopal, M. G. Haines, P. A. Norreys, U. Wagner, M.-S. Wei, M. Zepf, and K. Krushelnick, Measuring huge magnetic fields, Nature (London) **415**, 280 (2002).

[16] M. Murakami, J. J. Honrubia, K. Weichman, A. V. Arefiev, and S. V. Bulanov, Generation of megatesla magnetic fields by intense-laser-driven microtube implosions, Sci. Rep. **10**, 16653 (2020).

[17] D. Shokov, M. Murakami, and J. J. Honrubia, Laser scaling for generation of megatesla magnetic fields by microtube implosions, High Power Laser Sci. Eng. **9**, e56 (2021).

[18] L. D. Landau and E. M. Lifshitz, *The Classical Theory of Fields*, 4th ed. (Butterworth-Heinemann, Oxford, 1980).

[19] J. E. Gunn and J. P. Ostriker, On the motion and radiation of charged particles in strong electromagnetic waves. I. motion in plane and spherical waves, Astrophys. J. **165**, 523 (1971).

[20] A. A. Kolomenskii and A. N. Lebedev, Self-resonant particle motion in a plane electromagnetic wave, Sov. Phys. Dokl. **7**, 745 (1963).

[21] V. Y. Davydovskiĭ, Possibility of resonance acceleration of charged particles by electromagnetic waves in a constant magnetic field, Sov. Phys. JETP **16**, 629 (1963).

[22] Y. B. Zeldovich and A. F. Illarionov, Scattering of a strong wave by an electron in a magnetic field, Sov. Phys. JETP **34**, 467 (1972).

[23] V. Sagar, S. Sengupta, and P. K. Kaw, Radiation reaction effect on laser driven auto-resonant particle acceleration, Phys. Plasmas **22**, 123102 (2015).

[24] A. M. Beloborodov, Scattering of ultrastrong electromagnetic waves by magnetized particles, Phys. Rev. Lett. **128**, 255003 (2022).

[25] T. D. Arber, K. Bennett, C. S. Brady, A. Lawrence-Douglas, M. G. Ramsay, N. J. Sircombe, P. Gillies, R. G. Evans, H. Schmitz, and A. R. e. a. Bell, Contemporary particle-in-cell approach to laser-plasma modelling, Plasma Phys. Control. Fusion **57**, 113001 (2015).

[26] C. P. Ridgers, J. G. Kirk, R. Duclous, T. G. Blackburn, C. S. Brady, K. Bennett, T. D. Arber, and A. R. Bell, Modelling gamma-ray photon emission and pair production in high-intensity laser-matter interactions, J. Comput. Phys. **260**, 273 (2014).

[27] A. Y. Kryachko and M. D. Tokman, Electromagnetically induced transparency in a magnetized plasma during oblique propagation of radiation, Plasma Phys. Rep. **31**, 229 (2005).

[28] D. Teychenné, A. Giulietti, D. Giulietti, and L. A. Gizzi, Magnetically induced optical transparency of overdense plasmas due to ultrafast ionization, Phys. Rev. E **58**, R1245 (1998).

[29] M. S. Hur, J. S. Wurtele, and G. Shvets, Simulation of electromagnetically and magnetically induced transparency in a magnetized plasma, Phys. Plasmas **10**, 3004 (2003).

[30] D. Mandal, A. Vashistha, and A. Das, Electromagnetic wave transparency of X mode in strongly magnetized plasma, Sci. Rep. **11**, 14885 (2021).